Applied Catalysis B: Environmental 110 (2011) 33–39

Contents lists available at SciVerse ScienceDirect

Applied Catalysis B: Environmental

journal homepage: www.elsevier.com/locate/apcatb

Mechanistic analysis of direct N_2O decomposition and reduction with H_2 or NH_3 over RuO_2

Marta Santiago [a], Vita A. Kondratenko [b], Evgenii V. Kondratenko [b], Núria López [c,**], Javier Pérez-Ramírez [a,*]

[a] Institute for Chemical and Bioengineering, Department of Chemistry and Applied Biosciences, ETH Zurich, Wolfgang-Pauli-Strasse 10, HCI E 125, CH-8093, Zurich, Switzerland
[b] Leibniz-Institut für Katalyse e. V. an der Universität Rostock, Albert-Einstein-Strasse 29a, D-18059, Rostock, Germany
[c] Institute of Chemical Research of Catalonia (ICIQ), Av. Països Catalans 16, 43007, Tarragona, Spain

ARTICLE INFO

Article history:
Received 10 June 2011
Received in revised form 4 August 2011
Accepted 18 August 2011
Available online 25 August 2011

Keywords:
N_2O decomposition
RuO_2
Hydrogen
Mechanism
Temporal analysis of products
Density functional theory

ABSTRACT

The mechanisms of direct N_2O decomposition and N_2O reduction by H_2 or NH_3 on RuO_2 has been studied by means of steady-state catalytic tests at ambient pressure, transient experiments in a temporal analysis of products (TAP) reactor, and density functional theory (DFT) simulations. Bulk RuO_2 is very active for N_2O decomposition into N_2 and O_2, achieving full conversion at 723 K. According to the DFT calculations, coordinatively unsaturated ruthenium (Ru_{cus}) sites are active for the decomposition and oxygen elimination from the surface is rate-limiting step. When pre-reducing RuO_2 with H_2, the de-N_2O activity in the low-temperature region increases. This is attributed to the higher reactivity of surface oxygen vacancies created by H_2 at bridge sites compared to Ru_{cus} sites. Co-feeding of hydrogen or ammonia with nitrous oxide strongly accelerates the rate of N_2O elimination. TAP studies show that oxygen species formed upon N_2O decomposition over RuO_2 react with NH_3 and H_2 yielding N_2, NO, N_2O, and H_2O. Both TAP experiments and DFT simulations show that the N-containing intermediates coming from ammonia adsorb much stronger on the catalyst surface than H-containing intermediates coming from hydrogen. This causes blockage of active sites for N_2O decomposition by the former species, accounting for the higher efficiency of H_2 as reductant for N_2O. The presence of O_2 in the feed cancels the reducing effect of H_2 or NH_3 due to the more favorable re-oxidation of reduced RuO_2 by O_2 compared to N_2O.

1. Introduction

The development of catalytic technologies for N_2O abatement in the chemical industry constitutes one of the most prominent success stories of environmental catalysis in the last decade. A representative indicator is the large number of CDM (clean development mechanism) projects registered for N_2O mitigation in nitric acid, adipic acid, and caprolactam plants [1]. The pioneering review by Kapteijn et al. [2] set the path for the discovery and implementation of industrial de-N_2O catalysts such as iron-containing zeolites and mixed oxides with spinel (Co_2AlO_4/CeO_2) and perovskite ($La_{0.8}Ce_{0.2}CoO_3$) structures [3]. Common denominators of these catalytic systems, which operate in different temperature regimes, are high tolerance to inhibitors (namely O_2, NO_x, and H_2O) and long lifetime.

Supported ruthenium catalysts display a high activity for N_2O decomposition. Li and Armor [4] were among the first authors reporting the superior de-N_2O performance of Ru/ZSM-5, only exceeded by Rh/ZSM-5. Since then, various studies dealing with Ru-based catalysts have assessed the influence of the metal loading, the type of the support, the method for active phase deposition, the pre-treatment conditions, and the feed composition [5–12]. All the above supported systems decompose N_2O in the temperature range of 523–723 K. However, O_2, H_2O, NO, and SO_2 inhibit (or poison) the catalysts, limiting their practical application. Pirngruber et al. [13] showed that the inhibiting effect of NO is diminished when using a bi-metallic Fe-Ru/ferrierite material. Kawi et al. [8] reported the reduction of N_2O by CO over Ru/MCM-41. A full degree of N_2O conversion was achieved at 573 K in N_2O + CO mixtures, that is, 180 K lower temperature than for direct N_2O decomposition. The enhanced activity was attributed to the removal of adsorbed oxygen species formed upon nitrous oxide decomposition by carbon monoxide, leading to N_2 and CO_2. Komvokis et al. [11] confirmed

* Corresponding author. Tel.: +41 44 633 7120; fax: +41 44 633 1405.
** Corresponding author.
E-mail addresses: nlopez@iciq.es (N. López), jpr@chem.ethz.ch (J. Pérez-Ramírez).

0926-3373/$ – see front matter © 2011 Elsevier B.V. All rights reserved.
doi:10.1016/j.apcatb.2011.08.019

the high efficiency of CO as a reducing agent for N_2O in O_2-free mixtures over Ru/γ-Al_2O_3. On the other hand, discrepant conclusions have been reached concerning the catalyst pre-treatment. Pinna et al. [7] reported that Ru/ZrO_2 was more active in N_2O decomposition after pre-treatment under oxidizing atmosphere than under reducing atmosphere. Oppositely, Komvokis et al. [11] showed that a slightly higher rate of N_2O decomposition was attained after H_2 pre-treatment of Ru/γ-Al_2O_3. The same authors demonstrated that a H_2 treatment can be effectively used to regenerate the catalyst after N_2O decomposition in the presence of SO_2, O_2, and H_2O by means of cyclic reaction-reduction steps.

In contrast to the number of applied studies reporting de-N_2O performance of Ru-based catalysts under simulated off-gas conditions, fundamental understanding of the reaction on this metal oxide is limited. The low-temperature de-N_2O activity of ruthenium-containing materials is an interesting feature for sources of current concern, like surgery rooms of hospitals that use nitrous oxide as anesthetic agent [14]. At this stage, basic questions concerning the reaction mechanism can be formulated. Can we ascertain the cause for the different de-N_2O efficiency of RuO_2 in oxidized or reduced form? What is the best choice for a reducing agent in order to achieve low-temperature de-N_2O operation? Herein, we have investigated the mechanism of direct N_2O decomposition and N_2O reduction by NH_3 or H_2 over bulk RuO_2 at a molecular level. Continuous-flow catalytic tests at ambient pressure were combined with transient mechanistic studies by temporal analysis of products and density functional theory simulations.

2. Experimental

2.1. Catalytic tests

Anhydrous ruthenium(IV) oxide was purchased from Sigma Aldrich (99.9%). Prior to use, the as-received powder was calcined in static air at 773 K for 5 h using a heating rate of 10 K min^{-1}. Powder X-ray diffraction (XRD) confirmed the presence of RuO_2 (JCPDS 40-1290) as the only crystalline phase in the sample. The calcined sample possessed a total surface area of 10 $m^2\,g^{-1}$ (N_2 adsorption at 77 K).

The direct decomposition of N_2O and the reduction of N_2O with H_2 or NH_3 over RuO_2 were investigated in a fixed-bed continuous-flow tubular reactor made out of quartz (10 mm i.d.) at a total pressure of 1 bar. The catalyst (100 mg, particle size = 200–300 μm) was packed within the isothermal zone of the reactor between two layers of quartz wool and rested over a porous frit. The reactor was heated by an electrical furnace and the temperature was monitored by a thermocouple inside the catalyst bed. The catalyst was pre-treated at 673 K for 1 h in He or 5 vol.% H_2/He (50 ml STP min^{-1}) and cooled down in He to the initial reaction temperature (323 K). Then, He was replaced by the N_2O-containing mixtures and the temperature was increased at intervals of 50 K up to 723 K. An isothermal period ranging from 30 min to several hours was sustained at each set point to secure steady-state measurements. The catalytic performance at selected temperatures was re-measured on decreasing the temperature, enabling a comparison of up and down-temperature cycles. Feed mixtures contained N_2O (1.5 mbar), H_2 (1.5 mbar), NH_3 (1.5 mbar), and O_2 (1.5 mbar) in He. The total gas flow was 50 ml STP min^{-1}. The space time, defined as the ratio between the catalyst mass and the inlet molar flow of nitrous oxide was $W/F^o(N_2O) = 498\ g\,h\,mol^{-1}$. The degree of N_2O conversion was determined from inlet and outlet N_2O concentrations using an on-line gas chromatograph (SRA Instruments Micro-GC 3000) equipped with PLOT-Q column and TCD detector.

2.2. Transient experiments in vacuum

Direct N_2O decomposition and N_2O reduction by H_2 or NH_3 over RuO_2 were investigated in the Temporal Analysis of Products (TAP-2) reactor, a transient pulse technique operating in vacuum with sub-millisecond time resolution [15,16]. The sample (20 mg, particle size = 250–350 μm) was packed within the isothermal zone of the quartz micro-reactor (40 mm length, 6 mm i.d.) between two layers of quartz particles of the same particle size. The catalyst was pre-treated in flowing O_2 (20 ml STP min^{-1}) at 528 K and 1 bar for 30 min, followed by evacuation to 10^{-5} Pa at the same temperature. Direct N_2O decomposition was investigated by pulsing a mixture of N_2O:Ne = 1:1 (total pulse size = 5×10^{15} molecules) in the temperature range of 497–557 K at 15 K intervals, starting from 497 K. The ramping from one temperature to the next one was performed in vacuum. The catalyst was pre-treated at each temperature using large N_2O pulses (10^{16} molecules) in order to have it as re-oxidized as possible (RuO_2 could undergo partial reduction in vacuum). In order to derive mechanistic insights into N_2O reduction by H_2 (or NH_3), pump-probe experiments of N_2O:Ar = 1:1 and H_2:Xe = 1:1 (or $^{15}NH_3$:Xe = 1:1) were carried out at 523 K (548 K) with a time delay (Δt) of 0.5 s between the pulsed mixtures. The pulse size of the individual mixtures was the same as in direct N_2O decomposition experiments.

A quadrupole mass spectrometer (HAL RC 301 Hiden Analytical) was used for quantitative analysis of reactants and reaction products. The transient responses at the reactor outlet were monitored at the following atomic mass units (AMUs): 132 (Xe), 46 ($^{15}N_2O$), 44 (N_2O), Ar (40), 32 (O_2), 31 (^{15}NO), 30 (N_2O, NO, $^{15}N_2$), 28 (N_2, N_2O), 20 (Ne), 18 ($^{15}NH_3$, H_2O), and 2 (H_2). In the experiments, 10 pulses for each AMU were averaged in order to improve the signal-to-noise ratio. The concentrations of feed components and reaction products were determined from the corresponding AMUs using standard fragmentation patterns and sensitivity factors.

3. Computational details

Density functional theory (DFT) calculations were performed with the VASP code [17,18]. The functional employed was RPBE [19], and the inner electrons were replaced by PAW pseudopotentials [20], while the valence ones were expanded in plane waves with a maximum cut-off energy of 400 eV. The RuO_2 lattice was cut along the lowest energy surface (1 1 0) and a slab constituted by three layers of the Ru_2O_4 units was considered. In this case, the reconstruction employed was a $p(4 \times 1)$. To model the partially reduced surface, an atom from the bridge position of ruthenium oxide was removed generating a vacant site. The top layer of RuO_2 and the adsorbates' degrees of freedom were optimized in the simulations. The N_2O molecule was adsorbed on these layers in different configurations. The corresponding reaction profiles and energies for the dissociation and reduction processes were obtained. In addition, the surface reduction by H_2 and NH_3 was analyzed in detail together with O_2 adsorption. To locate transition state structures, the climbing image version of the Nudged Elastic Band, CI-NEB [21] was employed. *k*-point sampling was performed with the Monkhorst–Pack scheme [22] with meshes of $2 \times 4 \times 1$ for the oxide slabs. The frequencies were determined by numerically calculating the Hessian matrix, with two displacements of 0.02 Å for each adsorbate degree of freedom and then diagonalizing this matrix.

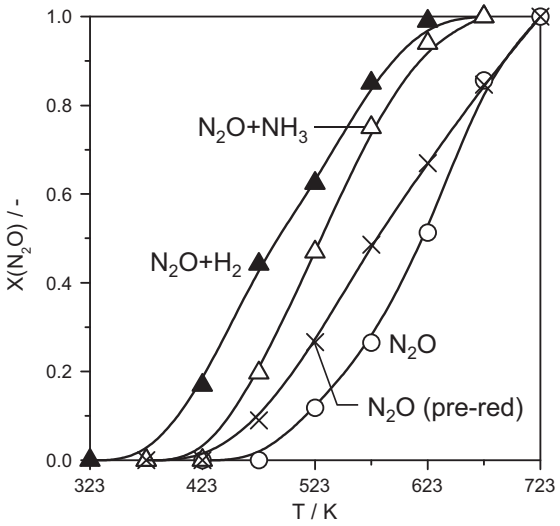

Fig. 1. Steady-state N_2O conversion versus temperature over RuO_2 in mixtures containing N_2O, NH_3, and H_2 (all components with a partial pressure of 1.5 mbar); balance He. The label 'pre-red' indicates that RuO_2 was pre-reduced at 673 K prior to evaluation in direct N_2O decomposition. Other conditions: $W/F^o(N_2O) = 498\ g\ h\ mol^{-1}$ and $P = 1$ bar.

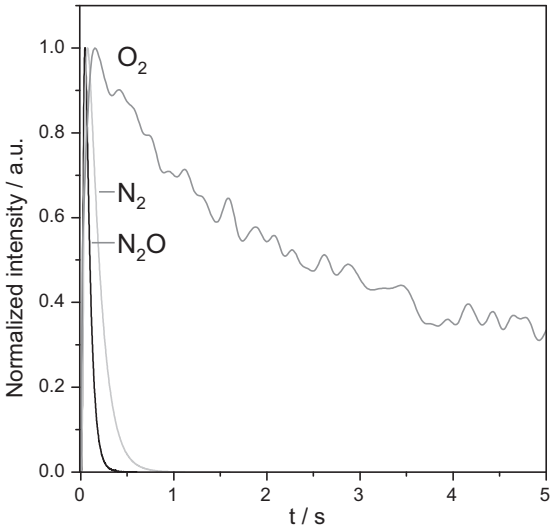

Fig. 2. Normalized transient responses of N_2O, N_2, and O_2 on pulsing of N_2O:Ne = 1:1 over RuO_2 at 497 K.

4. Results and discussion

4.1. Steady-state catalytic tests

Fig. 1 shows the N_2O conversion as a function of temperature over RuO_2 (pre-treated in He or H_2) in the absence and the presence of H_2 and NH_3 during continuous-flow catalytic tests at ambient pressure. The direct N_2O decomposition for the sample pre-treated in He starts above 473 K and reaches 100% conversion at 723 K. In agreement to Komvokis et al. [11], the pre-reduced sample exhibits a higher activity than the He pre-treated analogue, shifting the light-off to ca. 50 K lower temperature. The de-N_2O activity over RuO_2 increased upon co-feeding H_2 or NH_3. The addition of 1.5 mbar of H_2 shifted the conversion profile of direct N_2O decomposition by 100 K to lower temperature. The efficiency of ammonia as reducing agent for nitrous oxide was significantly lower compared to hydrogen. The N_2O conversion was very similar in up and down-temperature cycles with the above feed compositions or pre-treatments. It should be mentioned that when 1.5 mbar O_2 was co-fed with the $N_2O + H_2$ and $N_2O + NH_3$ mixtures, the N_2O conversion profile coincided to that of direct N_2O decomposition (not shown). This suggests that neither H_2 nor NH_3 are selective reducing agents for N_2O, that is, their reaction with O_2 is more favorable. However, when O_2 was removed from the feed mixture, the N_2O conversion increased reaching the original values. Mechanistic insights into the above observations are elaborated below on the basis of TAP and DFT analyses.

4.2. Temporal analysis of products

4.2.1. Direct N_2O decomposition

Fig. 2 compares the height-normalized responses of N_2O, N_2, and O_2 upon pulsing a mixture of N_2O:Ar = 1:1 over RuO_2 at 497 K. Following our previous approach [23], we analyzed the order of appearance and the shapes of these responses. The time of the maximal concentration (t_{max}) of N_2 (0.072 s) is halved to that of O_2 (0.150 s) at this temperature, but still significantly longer than the t_{max} value of N_2O (0.045 s). This is due to the fact that the reactant N_2O decomposes into N_2 and O_2. The difference of the t_{max} of N_2 and O_2 indicates that the reaction pathways leading to these products occur with substantially different rates; the overall rate of N_2 formation is much faster than that of O_2. Another important distinction between the transients of N_2 and O_2 is a long tailing (slow decrease in the product concentration with time) of the O_2 response. This tailing suggests that (i) the formed O_2 re-adsorbs over the catalyst and/or (ii) there might be several elementary reaction pathways leading to gas-phase O_2. Taking into account the results of DFT modeling elaborated below, we think that O_2 re-adsorption is the cause for the tailing. This implies that O_2 and N_2O compete for the same active sites, which agrees with the inhibiting effect of gas-phase O_2 on N_2O decomposition [2,4,8,24].

4.2.2. N_2O reduction

Pump-probe experiments with N_2O (pump molecule) and $^{15}NH_3$ or H_2 (probe molecules) were performed for deriving mechanistic insights into the N_2O decomposition in the presence of reducing agents. In this operation mode, N_2O was pulsed first followed after a delay of 0.5 s by a pulse of $^{15}NH_3$ (H_2). The overall duration of both pulses was 4 s. After this time, the pump and probe pulses were repeated at least 80 times, keeping constant both the overall time and the time delay. In contrast to simultaneous pulsing of N_2O and $^{15}NH_3$ (H_2) (i.e. time delay equal to zero), pump-probe experiments help to evaluate whether adsorbed oxygen species resulting from N_2O decomposition oxidize ammonia (hydrogen). Vice versa, one can evaluate whether nitrogen- and hydrogen-containing surface intermediates, which could be formed in the $^{15}NH_3$ and H_2 pulses and retained on the catalyst surface, are oxidized in the N_2O pulse. Isotopically labeled $^{15}NH_3$ and non-labeled N_2O were used to decouple the analysis of nitrous oxide and nitrogen from these feed components. Figs. 3 and 4 show non-normalized responses of feed components and reaction products detected in N_2O–$^{15}NH_3$ and N_2O–H_2 pump-probe experiments at 523 K, respectively. As expected, N_2 and O_2 were formed in the N_2O pulse. It is worth mentioning that the concentration of O_2 sharply decreased when either $^{15}NH_3$ or H_2 entered the reactor, proving that oxygen species formed from N_2O reacted with the reducing agents. The formation of $^{15}N_2O$, ^{15}NO, $^{15}N_2$, and H_2O in the $^{15}NH_3$ and H_2 pulses further supports this conclusion. This is also in agreement with DFT calculations (vide infra). From a selectivity viewpoint, the oxygen species formed from N_2O and lattice oxygen of RuO_2 perform very similarly because N_2 was also the main reaction product of ammonia oxidation in

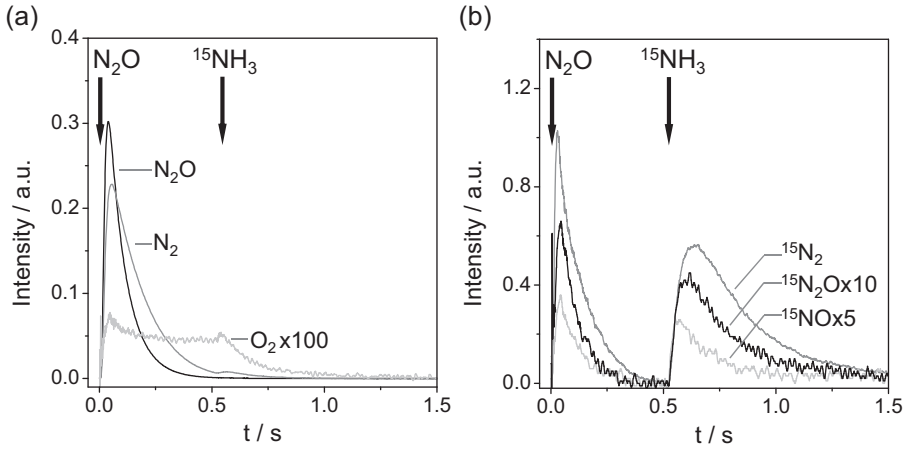

Fig. 3. Transient responses of (a) N_2O, N_2, and O_2 and (b) reaction products formed from $^{15}NH_3$ in pump-probe experiments of N_2O:Ar = 1:1 and $^{15}NH_3$:Xe = 1:1 at 523 K with a time delay of 0.5 s between the pulsed mixtures.

the absence of gas-phase O_2 [24]. When comparing the transient responses of N_2O and N_2 in Figs. 3 and 4, it can be seen that the N_2 response is higher than that of N_2O in the N_2O–H_2 experiments, while the situation is opposite in the N_2O–$^{15}NH_3$ experiments. This means that the conversion of N_2O in the presence of $^{15}NH_3$ is lower than in the presence of H_2 (40% versus 60%), in agreement with the outcome of continuous-flow tests at ambient pressure (Fig. 1).

Another important observation from Figs. 3 and 4 is the presence of $^{15}N_2O$, ^{15}NO, $^{15}N_2$ and H_2O in the N_2O pulse. This means that ^{15}N- and H-containing species remained on the catalyst surface after the $^{15}NH_3$ (H_2) pulses and reacted with nitrous oxide in the following pulse. In order derive insights into the adsorption strength of these species, we compared the amount of $^{15}N_2O$, ^{15}NO, $^{15}N_2$, and H_2O formed from $^{15}NH_3$ and H_2 in the N_2O pulse with the total amount of these products. It was estimated that only 5% of H_2O was formed in the N_2O pulse during the N_2O-H_2 experiments. Contrarily, approximately 30% of $^{15}N_2O$, ^{15}NO, and $^{15}N_2$ originated via oxidation of adsorbed ^{15}N-containing species in the N_2O pulse. These experimental results are in agreement with the DFT results of stronger NH_3 adsorption compared to that of H_2, which is elaborated in the next section. Therefore, we can put forward that the difference in the adsorption strength of these reducing agents is probably a reason for the distinctive effect of ammonia and hydrogen on N_2O reduction in Fig. 1.

4.3. Density functional theory

The mechanisms of N_2O decomposition on RuO_2 both in the absence and the presence of reducing agents were derived from DFT calculations. As shown in the insets of Fig. 5, we have employed different models for the RuO_2 surface: a regular RuO_2(1 1 0) and the same oxide presenting some surface vacancies, RuO_2:V_{Ob} All the relevant energy parameters are collected in Table 1.

4.3.1. Direct N_2O decomposition

N_2O can interact in different modes with the Ru-terminated RuO_2(1 1 0) surface. On this surface, N_2O is adsorbed on a Ru_{cus} (coordinatively unsaturated) atom in a configuration denoted as $N_{cus}NO$ by −0.26 eV (step 1, Table 1). In this configuration, the linear N_2O molecule is sitting N-down on Ru_{cus}. A second configuration, in which the terminal N and O atoms are in contact with two neighboring Ru_{cus} positions ($N_{cus}NO_{cus}$), is also possible (step 2, Table 1). The $N_{cus}NO_{cus}$ structure is about 0.58 eV higher in energy than $N_{cus}NO$ and is the precursor state for N_2O decomposition. The final products are O_{cus} and gas-phase N_2 (step 3, Table 1). The reaction is exothermic by 1.42 eV and the $N_{cus}NO_{cus}$ to $N_2 + O_{cus}$ barrier is 0.31 eV. At the transition state, the N–O distance is 1.491 Å. The oxygen atoms left on the surface can evolve to the gas phase in a two-step process. The first process has a barrier of 1.11 eV and results in an adsorbed O_{2cus} molecular species. The desorption of this

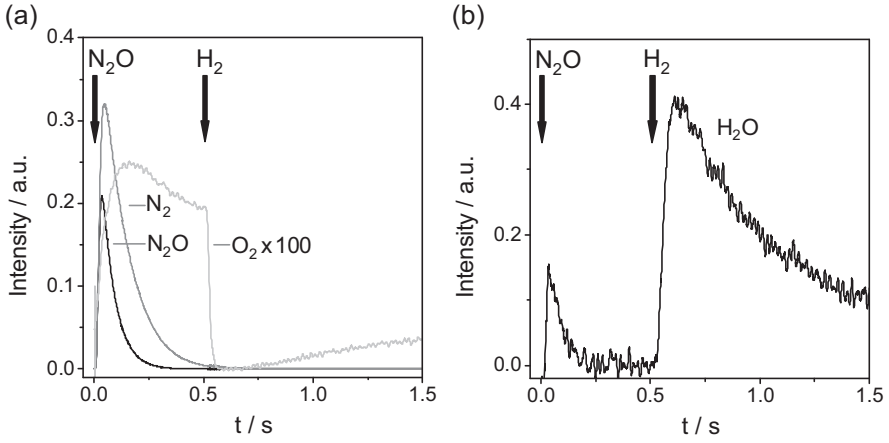

Fig. 4. Transient responses of (a) N_2O, N_2, and O_2 and (b) H_2O in pump-probe experiments of N_2O:Ar = 1:1 and H_2:Xe = 1:1 at 523 K with a time delay of 0.5 s between the pulsed mixtures.

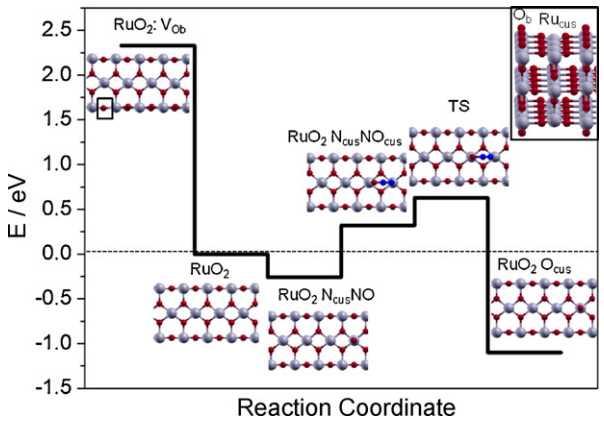

Fig. 5. Energy profile for N_2O decomposition on a regular and oxygen-deficient $RuO_2(1\,1\,0)$ surface. Large light blue spheres correspond to Ru atoms and dark red spheres stand for O atoms; the N atoms are represented by small dark blue spheres. The square indicates the position of the oxygen vacancy, V_{Ob}. Inset: schematic representation of the 3D model employed. (For interpretation of the references to color in this figure legend, the reader is referred to the web version of the article.)

precursor is endothermic by 0.67 eV (step 5, Table 1). Then it forms a molecular O_{2cus} species that can evolve to the gas phase; this reaction is endothermic by 0.67 eV (step 5, Table 1). Therefore, oxygen recombination is the most energy-demanding step for N_2O decomposition on $RuO_2(1\,1\,0)$. This is the reason why long tailings were found in the transient O_2 response (Fig. 2), as oxygen re-adsorption is a very likely process. The process is schematically shown in Fig. 6. The evolution of gas-phase O_2 is rate-determining step (indicated by dashed lines).

The oxygen-deficient $RuO_{2-x}(1\,1\,0)$ surface effectively catalyzes N_2O decomposition too. We considered the interaction of nitrous oxide with an anion surface vacancy (V_{Ob}), resulting in two possible adsorption configurations, i.e. N_bNO and NNO_b, where either the terminal N or O are filling the vacancy. In the first configuration, the adsorbate is molecularly bonded by −0.15 eV, whereas the

Table 1
Reaction energies (ΔE), activation barriers (E_a), and imaginary frequencies for the transition state structures (ν_i) of relevant elementary steps on $RuO_2(1\,1\,0)$.

#	Elementary step	ΔE (eV)	E_a (eV)	ν_i (cm^{-1})
1	$N_2O + *_{cus}$ [a] $\rightarrow N_{cus}NO$	−0.26		
2	$N_2O + 2*_{cus} \rightarrow N_{cus}NO_{cus}$	0.32		
3	$N_{cus}NO_{cus} \rightarrow N_2 + O_{cus} + *_{cus}$	−1.42	0.31	534
4	$2O_{cus} \rightarrow O_{2cus} + *_{cus}$	0.50	1.11	585
5	$O_2 + 2*_{cus} \rightarrow O_{2cus}$	0.67		
6	$N_2O + V_{Ob}$ [b] $\rightarrow O_b + N_2$	−2.67		
7	$H_2 + *_{cus} \rightarrow H_{2cus}$	0.10		
8	$H_{2cus} + O_b \rightarrow H_{cus} + O_bH$	−0.66	0.43	868
9	$H_{cus} + O_bH \rightarrow H_2O_b$	0.17/0.01	1.11/0.44	1277/1081
10	$H_2O_b \rightarrow H_2O + V_{Ob}$	0.47		
11	$H_{2cus} + O_{cus} \rightarrow H_{cus} + O_{cus}H$	−0.77	0.37	1051
12	$O_bH + O_{cus}H \rightarrow H_2O_{cus} + O_b$	−1.50	0.64	748
13	$H_2O_{cus} \rightarrow H_2O + *_{cus}$	0.47		
14	$NH_3 + *_{cus} \rightarrow NH_{3cus}$	−1.15		
15	$NH_3{*_{cus}} + O_b \rightarrow NH_{2cus} + O_bH$	0.48	0.57	394
16	$NH_2{*_{cus}} + O_b \rightarrow NH_{cus} + O_bH$	0.45	0.85	1430
17	$NH{*_{cus}} + O_b \rightarrow N_{cus} + O_bH$	−0.93	0.07	211
18	$2N{*_{cus}} \rightarrow N_2 + *_{cus}$	−3.41	1.11	647
19	$O_2 + 2*_{cus} \rightarrow O_{2cus}$	−0.67		
20	$O_{2cus} + *_{cus} \rightarrow 2O_{cus}$	−0.50	0.61	585
21	$O_2 + V_{Ob} \rightarrow O_2@V_{Ob}$ [c]	−1.38		
22	$O_2@V_{Ob} + *_{cus} \rightarrow O_b + O_{cus}$	−1.56	0.24	304

[a] $*_{cus}$: free Ru_{cus} site.
[b] V_{Ob}: oxygen vacancy at a bridge position of $RuO_2(1\,1\,0)$.
[c] $O_2@V_{Ob}$ stands for an oxygen molecule sitting at a vacancy site on the surface.

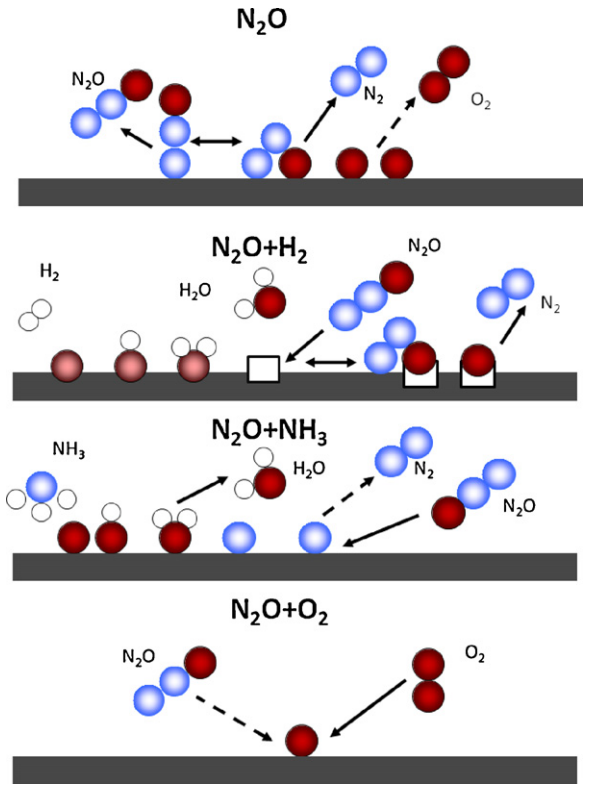

Fig. 6. Schematic representation of the reactions with different initial mixtures. The arrows indicate possible processes, squares oxygen vacancies, light blue spheres N, small white spheres H, dark red spheres O. Unlikely events are marked by discontinuous lines. (For interpretation of the references to color in this figure legend, the reader is referred to the web version of the article.)

second one spontaneously decomposes yielding gas-phase N_2 and healing the oxygen vacancy (O_b). The latter process is very exothermic by 2.67 eV (step 6, Table 1). Based on these results, it can be concluded that oxygen vacancies at the bridge rows of RuO_2 (V_{Ob}) are highly active sites for N_2O decomposition. This may explain the higher N_2O decomposition activity of pre-reduced RuO_2 in the low-temperature region (Fig. 1), which is in line with previous studies [11].

4.3.2. N_2O reduction by H_2 or NH_3

H_2 weakly adsorbs on Ru_{cus} sites and reacts with bridged oxygen (O_b) species through the steps 7–13 in Table 1. H_2 adsorption on ruthenium dioxide was computed in a previous study [25]. The H_2 binding energy to Ru_{cus} is endothermic by 0.10 eV and the H–H distance is 0.786 Å. O_b can act as H attractor and thus promote H_2 dissociation. The activation energy for O_bH formation is 0.43 eV. The O_b–H distance at the transition state is 1.498 Å, while the H–H distance is 0.915 Å. The final distances for O_b–H and H–Ru_{cus} are 0.984 and 1.640 Å, respectively. The reaction is exothermic by 0.66 eV (step 8, Table 1). The second H atom can be transferred to the O_bH group to form a water molecule at O_b positions. This reaction consists of two steps (step 9, Table 1); the proton initially moves to the fully coordinated oxygen at the surface and then to the O_bH. The total reaction energy is $\Delta E = 0.18$ eV, and the activation energies for the elementary steps are, $E_a = 1.11$ and 0.44 eV, respectively. The elimination of H_2O_b requires 0.47 eV, leading to an anion vacancy formed at the bridge position (V_{Ob}) (step 10, Table 1). However, the overall reaction $H_2 + O_b \rightarrow V_{Ob} + H_2O$ is exothermic by 0.49 eV. When oxygen atoms are present at the cus site (O_{cus}), the adsorption of H_2 is more favorable. H_2 dissociation occurs through a similar path as the one described for the O_b site. However, the

energy requirements to form H_2O_{cus} are lower than in the previous case, with barriers of 0.37 and 0.64 eV for the first and second H transfer processes, respectively (steps 11 and 12, Table 1). The elimination of H_2O_{cus} requires 0.47 eV (step 13, Table 1). In this case, the full reaction energy for $H_2 + O_{cus} \rightarrow H_2O$ is exothermic by 2.35 eV, while for the oxygen at bridge positions is practically thermoneutral ($H_2 + O_b \rightarrow H_2O$, $\Delta E = 0.09$ eV).

Contrarily to hydrogen, ammonia strongly adsorbs on the RuO_2(1 1 0) surface. The adsorption energy is above 1 eV (step 14, Table 1). Adsorbed ammonia can be dehydrogenated through steps 15–17 in Table 1. The first barrier for H stripping is 0.57 eV and is endothermic by 0.48 eV. The two following reaction steps for complete NH_3 dehydrogenation are endothermic and have activation energies of 0.85 eV (step 16, Table 1) and 0.07 eV (step 17, Table 1). However, after water evolution is completed, N atoms are still bound to Ru_{cus} sites. Although nitrogen elimination as N_2 is highly exothermic (3.41 eV), it is hindered by a relatively large barrier of 1.11 eV (step 18, Table 1). Therefore, this step is rate limiting (dashed line in Fig. 6). The formation and desorption of NO is even more energetically demanding [24].

With the above results, it is possible to compare the ability of ammonia and hydrogen to reduce the RuO_2(1 1 0) surface. The thermodynamics for the reduction processes taking place in the experiments of Figs. 3 and 4 can be written as follows:

$$H_2 + RuO_2 \rightarrow RuO_2{:}\,V_{Ob} + H_2O \quad \Delta E = -0.01\ \text{eV}$$

$$NH_3 + RuO_2 \rightarrow RuO_2{:}\,V_{Ob} + 1.5H_2O + 0.5\,N_2 \quad \Delta E = -2.91\ \text{eV}$$

where RuO_2:V_{Ob} corresponds to the RuO_2 from which a bridge oxygen atom has been removed. The reduction by H_2 is close to thermo-neutral, while the reduction by NH_3 is strongly exothermic due to the formation of the triple bond in N_2, Based on this, ammonia should be more prone to form vacancies on the RuO_2 surface. However, the kinetic regime of these two reactions is quite different. Indeed, the largest barriers for the formation of oxygen vacancies on RuO_2(1 1 0) via reaction with H_2 and NH_3 are about 0.6 eV and 1 eV, respectively (step 12 versus step 18 in Table 1). Therefore, upon reaction with ammonia, a sizeable amount of N-containing fragments can populate Ru_{cus} positions. These fragments block N_2O adsorption and dissociation since ammonia adsorption is thermodynamically preferred (step 14, Table 1). In comparison, the binding energy of both N_2O and H_2 on the surface is very weak and comparable (step 1 and 7, Table 1). Thus, hydrogen-related moieties do not block active sites for N_2O decomposition on the RuO_2 surface.

Indeed, the presence of adsorbed hydrogen can help the reaction in two different ways (Fig. 6). If the surface is pre-treated with H_2 a certain number of oxygen vacancies at the bridge sites, V_{Ob}, can be created following the path described earlier. These sites are more prone to dissociate N_2O by healing the vacancy with the incoming molecule. However, the N_2O conversion profile of the H_2 pre-treated RuO_2 did not decrease to the profile of the He pre-treated RuO_2 on several up and down-temperature cycles in the N_2O-containing feed mixture. Therefore, pre-reduction of ruthenium dioxide causes a permanent transformation of the active sites and/or defect chemistry of RuO_2. Further studies would be required to identify differences in the active sites of RuO_2 and pre-reduced RuO_2 after a long exposure to N_2O. In addition to the generation of vacancies, the simultaneous presence of N_2O and H_2 can accelerate decomposition as hydrogen-containing products would preferentially transfer protons to oxygen atoms at the cus sites. Once fully hydrogenated, the O_{cus} atoms can evolve as H_2O instead of O_2. As the H-assisted route is energetically more favored (the most energy demanding steps are 0.64 eV for the H-assisted route versus 1.11 eV for the H-free route, see steps 12 and 4 in Table 1), the presence of H_2 in the feed mixture boosts the de-N_2O activity. The lower light-off temperature in the $N_2O + H_2$ experiments compared to the H_2 pre-reduction strongly suggests that (i) the N_2O decomposition route taking place at the reduced sites can proceed in a sustained manner and that (ii) there is a side route in which H atoms can remove other oxygen intermediates on the surface.

Finally, the high efficiency of CO for N_2O reduction over RuO_2-based catalysts reported elsewhere [8,11] can be explained attending to previous theoretical results. Reuter et al. [26] have shown that CO can eliminate oxygen atoms at cus positions and eventually even O_b atoms to generate vacancies. The energy required for these processes is 0.9 eV ($CO_{cus} + O_{cus} \rightarrow CO_2 + 2^*$ and 1.2 eV ($CO_{cus} + O_b \rightarrow CO_2 + {}^* + V_{Ob}$), while the CO binding energy is exothermic by about 1.31 eV (PBE functional). Therefore, the ability of CO to sweep out O_{cus} atoms coming from the decomposition of N_2O or to generate V_{Ob} is likely to be midway between that of H_2 and NH_3, as the binding energy of CO is large. However, CO is easier to eliminate through reaction with surface oxygen than nitrogen by recombination to N_2.

4.3.3. Influence of O_2

Adsorption of molecular oxygen occurs easily at different surface Ru_{cus} positions. For comparative purposes, we have investigated the interaction at both Ru_{cus} (steps 19–20, Table 1) and oxygen vacancies (V_{Ob}) generated after reduction processes. The reader should notice that steps 19 and 20 correspond to the inverse of steps 4 and 5 and are only listed separately to ease the discussion. A stable molecular configuration characterized by a O–O distance of 1.317 Å was found at regular RuO_2 surfaces on top Ru_{cus} sites (step 19, Table 1). This structure constitutes a precursor for the complete dissociation of O_2 into two O_{cus} atoms. The barrier for this process is 0.61 eV and the reaction energy is −1.21 eV (with respect to gas-phase O_2, step 20 in Table 1). Therefore, O_2 dissociation is rather easy on the RuO_2 surface in agreement with previous DFT calculations [27]. On the oxygen-deficient RuO_{2-x} surface, O_2 can be adsorbed at the oxygen bridge vacancy (steps 20–21, Table 1). For this process, the binding energy is −1.38 eV and the O–O distance is 1.321 Å. O_2 dissociation results in vacancy healing and O_{cus} formation. The reaction is exothermic by 1.56 eV. Therefore N_2O decomposition dramatically changes in the presence of gas-phase O_2 (Fig. 6). N_2O and O_2 have very different adsorption energies on the RuO_2(1 1 0) surface. O_2 is by far preferred on the surface. The total adsorption energy, upon dissociation is 1.17 eV to be compared to 0.26 eV for N_2O (steps 21–22 versus step 1 in Table 1). Preferential adsorption (thermodynamic selectivity) is the major control in the reactivity of mixtures. Therefore, the selectivity of RuO_2(1 1 0) towards N_2O:O_2 mixtures is very small due to the competitions for active sites.

5. Conclusions

Bulk RuO_2 is a highly active catalyst for N_2O decomposition into N_2 and O_2. The catalyst in reduced form (by H_2) exhibits a higher activity at low temperature, due to the higher reactivity of surface oxygen vacancies created by H_2 at bridge sites compared to coordinatively unsaturated ruthenium sites. The direct N_2O decomposition is limited by oxygen desorption, while the N_2O dissociation step to N_2 and adsorbed atomic oxygen presents a very low barrier. The use of agents such as NH_3 and H_2 assists the reduction of the surface. Hydrogen is more effective than ammonia due to the strong adsorption of NH_3-derived intermediates, which block active sites for N_2O dissociation. Unfortunately, the reducing agents are not selective for N_2O in the presence of O_2. The major reason for this behavior is related to the high affinity of oxygen for the

active sites on the RuO_2 surface that block N_2O adsorption by thermodynamic selectivity. Therefore the thermodynamic selectivity accounts for both the competition between N_2O and oxidants as O_2 or reductants as NH_3.

Acknowledgements

We thank ETH Zurich, MICINN (Consolider Ingenio 2010 CSD2006-003, CTQ2009-07553/BQU) and BSC-RES.

References

[1] S.-J. Lee, I.-S. Ryu, B.-M. Kim, S.-H. Moon, Int. J. Greenh. Gas Control 5 (2011) 167.
[2] F. Kapteijn, J. Rodríguez-Mirasol, J.A. Moulijn, Appl. Catal. B 9 (1996) 25.
[3] J. Pérez-Ramírez, F. Kapteijn, K. Schöffel, J.A. Moulijn, Appl. Catal. B 44 (2003) 117.
[4] Y. Li, J.N. Armor, Appl. Catal. B 1 (1992) L21.
[5] K. Li, X.F. Wang, H.C. Zeng, Trans. IChemE 75 (1997) 807.
[6] H.C. Zeng, X.Y. Pang, Appl. Catal. B 13 (1997) 113.
[7] F. Pinna, M. Scarpa, G. Strukul, E. Guglielminotti, F. Boccuzzi, M. Manzoli, J. Catal. 192 (2000) 158.
[8] S. Kawi, S.Y. Liu, S.-C. Shen, Catal. Today 68 (2001) 237.
[9] G.E. Marnellos, I.A. Vasalos, E.A. Efthimiadis, Appl. Catal. B 46 (2003) 523.
[10] P.S.S. Reddy, N. Pasha, M.G.V. Chalapathi Rao, N. Lingaiah, P.S. Suryanarayana, S. Prasad, Catal. Commun. 8 (2007) 1406.
[11] V.G. Komvokis, G.E. Marnellos, I.A. Vasalos, K.S. Triantafyllidis, Appl. Catal. B 89 (2009) 627.
[12] V.G. Komvokis, M. Marti, A. Delimitis, I.A. Vasalos, K.S. Triantafyllidis, Appl. Catal. B 103 (2011) 62.
[13] G.D. Pirngruber, L. Frunz, J.A.Z. Pieterse, J. Catal. 243 (2006) 340.
[14] Y. Tateishi, T. Tsuneyuki, H. Furukawa, H. Kagawa, I. Moriguchi, Y. Kanmura, Y. Teraoka, Catal. Today 139 (2008) 59.
[15] J.T. Gleaves, G.S. Yablonsky, P. Phanawadee, Y. Schuurman, Appl. Catal. A 160 (1997) 55.
[16] J. Pérez-Ramírez, E.V. Kondratenko, Catal. Today 121 (2007) 160.
[17] G. Kresse, J. Hafner, Phys. Rev. B 47 (1993) 55.
[18] G. Kresse, J. Furthmüller, Phys. Rev. B 54 (1996) 11169.
[19] B. Hammer, L.B. Hansen, J.K. Nørskov, Phys. Rev. B 59 (1999) 7413.
[20] G. Kresse, D. Joubert, Phys. Rev. B 59 (1999) 1758.
[21] G. Henkelman, B.P. Uberuaga, H. Jónsson, J. Chem. Phys. 113 (2000) 9901.
[22] H.J. Monkhorst, J.D. Pack, Phys. Rev. B 13 (1976) 5188.
[23] E.V. Kondratenko, V.A. Kondratenko, M. Santiago, J. Pérez-Ramírez, J. Catal. 256 (2008) 248.
[24] J. Pérez-Ramírez, N. López, E.V. Kondratenko, J. Phys. Chem. C 114 (2010) 16660.
[25] J. Wang, Y.F. Chao, Q. Sun, K. Reuter, K. Jacobi, M. Scheffler, G. Ertl, Angew. Chem. Int. Ed. 42 (2003) 2151.
[26] K. Reuter, D. Frenkel, M. Scheffler, Phys. Rev. Lett. 93 (2004) 116105.
[27] H. Wang, W.F. Schneider, D. Schmidt, J. Phys. Chem. C 113 (2009) 15266.